Available online at www.sciencedirect.com
SCIENCE DIRECT®
Journal of Molecular Spectroscopy 228 (2004) 441–452
Journal of MOLECULAR SPECTROSCOPY
www.elsevier.com/locate/jms

New analysis of the Coriolis-interacting v_2 and v_5 bands of $CH_3{}^{79}Br$ and $CH_3{}^{81}Br$

F. Kwabia Tchana,[a,d,*] I. Kleiner,[a] J. Orphal,[a] N. Lacome,[b] and O. Bouba[c]

[a] *Laboratoire de Photophysique Moléculaire, Bât. 350, 91405 Orsay Cedex, France*
[b] *Laboratoire de Dynamique, Interactions et Réactivité, Université Pierre et Marie Curie, UMR CNRS 7075, Case Courrier 49, 4 Place Jussieu, 75252 Paris Cedex 05, France*
[c] *Faculté des Sciences, Université de Ngaoundéré, B.P. 454 Ngaoundéré, Cameroon*
[d] *Centre de Physique Atomique Moléculaire et Optique Quantique (CEPAMOQ), Université de Douala, B.P. 8580 Douala, Cameroon*

Received 25 February 2004; in revised form 20 May 2004
Available online 28 July 2004

Abstract

The v_2 (A_1) and v_5 (E) fundamental bands of $CH_3{}^{79}Br$ and $CH_3{}^{81}Br$ have been studied by Fourier transform infrared spectroscopy with an unapodized resolution of $0.004\,cm^{-1}$, corresponding to an improvement of one order of magnitude compared to previous studies. For both isotopomers, some 2427 (2239) lines were newly assigned for the parallel and the perpendicular bands and, in addition, 80 perturbation-allowed transitions were also added. The ground-state axial rotational constants A_0 were redetermined from allowed and perturbation-allowed infrared transitions observed in the v_2 and v_5 bands around the local crossing. The A_0 values obtained for both isotopomers are more accurate but fully compatible with those obtained previously. Using those results, and the variation of the rotational constants with vibration, new accurate equilibrium constants A_e and B_e have been also determined for $CH_3{}^{79}Br$ and $CH_3{}^{81}Br$. The excited states $v_2 = 1$ and $v_5 = 1$ are coupled by Coriolis-type interactions ($\Delta l = \pm 1, \Delta K = \pm 1$) and ($\Delta l = \mp 1, \Delta K = \pm 2$), while the $l_5 = \pm 1$ levels of v_5 interact also through "$l(2,2)$"-type interaction ($\Delta l = \pm 2, \Delta K = \pm 2$). The Coriolis coupling term was determined to be $\zeta_{2,5} = 0.6121$ (6) for $CH_3{}^{79}Br$ and $\zeta_{2,5} = 0.6124$ (5) for $CH_3{}^{81}Br$. All interaction parameters have been determined with higher accuracy, compared to previous studies. A total of 4213 (3704) line positions with $J \leqslant 68$ (64) and $K \leqslant 16$ (11) including all available data was fitted using 20 (18) parameters with a root-mean-square deviation of 0.0007 (0.0006) cm^{-1} for $CH_3{}^{79}Br$ and $CH_3{}^{81}Br$, respectively. Two different but equivalent forms of reduced Hamiltonians with two different sets of constrained constants were successfully applied according to Lobodenko's reduction [J. Mol. Spectrosc. 126 (1987) 159]. The ratio of the transition moments, $|d_2/d_5| = 1.65$, and a positive sign of the Coriolis intensity perturbation $d_2 \times \zeta_{25} \times d_5$ were determined. Therefore, it has been possible to generate an accurate prediction of the whole spectrum between 1200 and $1650\,cm^{-1}$, including Q branches.

Keywords: Methyl bromide; Coriolis interaction; Resonance; High resolution; IR absorption

1. Introduction

Although brominated species are less abundant in the stratosphere than chlorinated ones, their role in the destruction of stratospheric ozone cannot be neglected because: (i) bromine is more efficient than chlorine in the depletion of ozone and (ii) brominated molecules can be more easily photodissociated than the chlorine analogues.

Methyl bromide, CH_3Br, has been identified as one of the major sources of atmospheric bromine. Methyl bromide has both natural and anthropogenic origins. Its known sources include natural production from oceans [1] and biomass burning [2]. It is also industrially produced for use in agricultural applications and structural fumigations. The tropospheric mixing

* Corresponding author. Fax: +33-1-69-15-75-30.
E-mail address: fridolin.kwabia@ppm.u-psud.fr (F. Kwabia Tchana).

0022-2852/$ - see front matter © 2004 Elsevier Inc. All rights reserved.
doi:10.1016/j.jms.2004.05.011

ratio of CH_3Br is 9–11 pptv in the Northern Hemisphere and about 8 pptv in the Southern Hemisphere, with an increase of about 0.15 pptv per year [3]. However, enhancements of CH_3Br in the Arctic and sub-Arctic lower troposphere during spring are still unexplained [4]. Clearly, measurements of atmospheric CH_3Br concentrations with sufficient spatial coverage to identify sources and sinks are required. Spectroscopy using satellite borne instruments can potentially be used for this task. For this, accurate modeling of the infrared spectrum of CH_3Br, including line intensities, is indispensable.

It is well known that in methyl halides, both in CH_3X and CD_3X, an *xy*-Coriolis interaction exists between the rovibrational levels of the states $v_2 = 1$ and $v_5 = 1$. The basic theory of the Coriolis resonance has been first presented by Di Lauro and Mills [5], who applied it to the interpretation of the v_2 and v_5 bands of CH_3F and CD_3Cl. As was pointed out later by Morino and Hirose [6], the same type of resonance is observed in the v_2 and v_5 bands of CH_3Br.

There have been various investigations in the past on the infrared and microwave spectra of methyl bromide. An extensive review of this molecule was given by Graner [7]. The most recent infrared work on this molecule was published in 2002 by Brunetaud et al. [8]. In that work, high-resolution spectra of the v_6 band of CH_3Br between 820 and 1120 cm^{-1} were recorded and line positions and intensities were predicted for atmospheric remote-sensing applications.

Two previous studies deal with the $v_2 = 1$ and $v_5 = 1$ states of CH_3Br. Graner and Blass [9] used infrared spectra at low resolution and therefore obtained first parameters, taking into account only the *xy*-Coriolis interaction. Anttila et al. [10] measured about 2990 rovibrational transitions in v_2 (centered around 1305.9 cm^{-1}) and v_5 (centered around 1442.9 cm^{-1}), with J up to 57, and fitted them by taking into account the Coriolis and "$l(2,2)$" interactions. In 1989, Ouahman et al. [11] published an infrared spectroscopic study at higher wavenumbers, between 1520 and 1700 cm^{-1} involving the combination band $v_3 + v_6$ and high values of K (7–16) of the v_5 band of $CH_3{}^{79}Br$. In that work, a model taking into account the "$l(2,2)$" resonance of v_5 and the Coriolis resonance between v_5 and v_2 was used. However, these authors did not see any evidence for interaction between $v_3 + v_6$ and v_5. About 74 lines of the v_2 band, taken from [10], combined with 577 lines of v_5 and 443 lines of $v_3 + v_6$ were used in [11].

In all these previous studies, no complete prediction involving line positions and intensities in the 1200–1650 cm^{-1} spectral range was available.

In the present work, we have completed the previous studies with some 2427 (2239) new assignments for $CH_3{}^{79}Br$ and $CH_3{}^{81}Br$, respectively, extending the range of the quantum number. We are thus able to report a complete prediction of line positions and intensities for $CH_3{}^{79}Br$ and $CH_3{}^{81}Br$ between 1200 and 1650 cm^{-1} accurate enough to determine optimal spectral windows for future atmospheric detection of CH_3Br.

2. Experimental details

A Bruker IFS 120 HR interferometer equipped with a globar source and a CaF_2/Si beam splitter was used. The spectra are recorded with an unapodized spectral resolution of 0.004 cm^{-1} which is significantly better than previous recordings in the same region [9,10]. A HgCdTe detector cooled by liquid nitrogen was used in conjunction with an optical filter, with a bandpass of 900–2000 cm^{-1} to improve the S/N ratio. A path length of 27.0 ± 0.1 cm and a CH_3Br pressure of 4.693 ± 0.005 mbar were chosen, and the cell was equipped with CaF_2 windows. All spectra were recorded at room temperature (296 ± 1 K) and spectral calibration was achieved by using water vapour absorptions. Thirty-six lines of H_2O between 1200 and 1650 cm^{-1} were applied, taking the reference wavenumbers from [12]. The spectral calibration is accurate to 1.6×10^{-4} cm^{-1} (RMS). Due to the good signal/noise (~350), even weak lines with low J and K values are observed. Overviews of the entire v_2 band and of the central region of the v_5 band of CH_3Br are shown in Figs. 1 and 2.

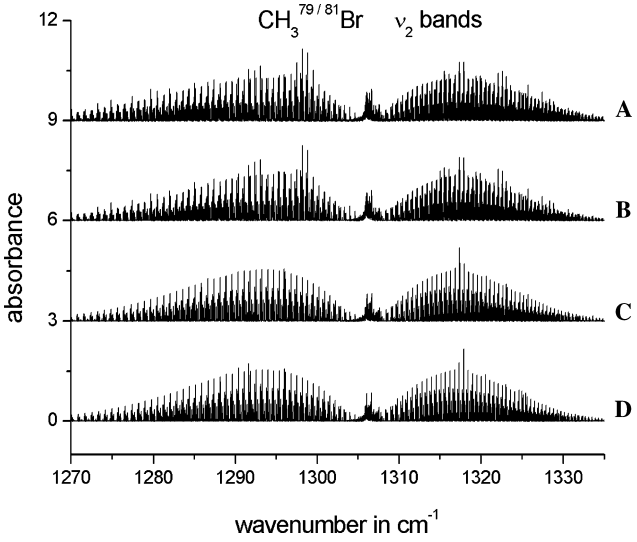

Fig. 1. Overview spectra of the v_2 bands of $CH_3{}^{79}Br$ and $CH_3{}^{81}Br$: (A) observed spectrum, recorded with a spectral resolution of 0.004 cm^{-1}, an optical path length of 27.0 ± 0.1 cm, at a pressure of 4.693 ± 0.005 mbar of CH_3Br and at room temperature. (B) Synthetic spectrum including both isotopomers, obtained by using the parameters of Model I. (C) Synthetic spectrum, $CH_3{}^{79}Br$ only. (D) Synthetic spectrum, $CH_3{}^{81}Br$ only.

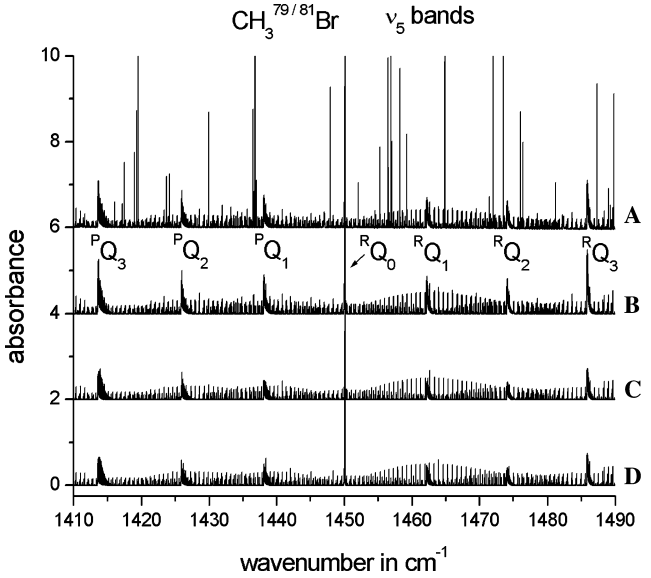

Fig. 2. The central region of the v_5 bands of $CH_3{}^{79}Br$ and $CH_3{}^{81}Br$, around 1410–1490 cm^{-1}. Experimental conditions as in Fig. 1. Assignments of the different Q branches are indicated. Note the presence of strong residual water lines in the observed spectrum (A), most of them have been used for calibration. (B) Synthetic spectrum including both isotopomers, obtained by using the parameters of Model I. (C) Synthetic spectrum, $CH_3{}^{79}Br$ only. (D) Synthetic spectrum, $CH_3{}^{81}Br$ only.

3. Theoretical model

The $v_2 = 1$ (A_1) and $v_5 = 1$ (E) vibrational levels of $CH_3{}^{79}Br$ and $CH_3{}^{81}Br$ are interacting through a Coriolis-type interaction. The levels are linked by ($\Delta l = \pm 1, \Delta K = \pm 1$) and ($\Delta l = \mp 1, \Delta K = \pm 2$) interactions, while the $l_5 = \pm 1$ levels of v_5 also interact by ($\Delta l = \pm 2, \Delta K = \pm 2$) interaction. The models used in this work, with 20 (18) floated parameters for $CH_3{}^{79}Br$ and $CH_3{}^{81}Br$, respectively, take into account all these resonances.

The rotational energy for the ground-state rotational energy levels may be written

$$\begin{aligned} E_0(J,K) = {} & B_0 J(J+1) + (A_0 - B_0)K^2 - D_J^0 J^2(J+1)^2 \\ & - D_{JK}^0 J(J+1)K^2 - D_K^0 K^4 + H_J^0 J^3(J+1)^3 \\ & + H_{JK}^0 J^2(J+1)^2 K^2 + H_{KJ}^0 J(J+1)K^4 + H_K^0 K^6. \end{aligned} \tag{1}$$

Analogously, the A_1 (nondegenerate) excited-state energy of $v_s = 1$, with $s = 2$, is calculated according to the formula:

$$\begin{aligned} E(v_s,J,K) = {} & v_s^0 + B_s J(J+1) + (A_s - B_s)K^2 \\ & - D_J^s J^2(J+1)^2 - D_{JK}^s J(J+1)K^2 \\ & - D_K^s K^4 + H_J^s J^3(J+1)^3 + H_{JK}^s J^2(J+1)^2 K^2 \\ & + H_{KJ}^s J(J+1)K^4 + H_K^s K^6. \end{aligned} \tag{2}$$

For the $v_t = 1$ degenerate (E) upper state, with $t = 5$, the diagonal matrix elements of the vibration–rotation Hamiltonian are [13]

$$\begin{aligned} E(v_t,l,J,K) = {} & v_t^0 + B_t J(J+1) + (A_t - B_t)K^2 \\ & - 2(A\zeta)_t Kl - D_J^t J^2(J+1)^2 \\ & - D_{JK}^t J(J+1)K^2 - D_K^t K^4 + H_J^t J^3(J+1)^3 \\ & + H_{JK}^t J^2(J+1)^2 K^2 + H_{KJ}^t J(J+1)K^4 \\ & + H_K^t K^6 + \eta_J J(J+1)Kl + \eta_K K^3 l, \end{aligned} \tag{3}$$

where $l = \pm 1$.The off-diagonal elements of the essential resonances "l"-type ($\Delta l = \pm 2, \Delta K = \pm 2$) and ($\Delta l = 0$, $\Delta K = \pm 3$) interactions within $v_5 = 1^{\pm 1}$ are taken as [14]:

$$\langle v_5,l,J,K|H|v_5,l\pm 2,J,K\pm 2\rangle = 2q_5 F_\pm(J,K)F_\pm(J,K\pm 1) \tag{4}$$

and

$$\begin{aligned} & \langle v_5,l,J,K|H|v_5,l,J,K\pm 3\rangle \\ & \quad = d_3 l F_\pm(J,K)F_\pm(J,K\pm 1)F_\pm(J,K\pm 2), \end{aligned} \tag{5}$$

where $F_\pm(J,K) = [J(J+1) - K(K\pm 1)]^{1/2}$.

We also took into account the Coriolis interaction of first order ($\Delta l = \pm 1, \Delta K = \pm 1$) between the $v_2 = 1$ and $v_5 = 1^{\pm 1}$ levels:

$$\begin{aligned} & \langle v_2 = 1, v_5 = 0, J, K|H|v_2 = 0, v_5 = 1, J, l = \pm 1, K\pm 1\rangle \\ & \quad = \sqrt{2}\Big[C_{11}^{(1)} + C_{11}^{(3a)}J(J+1) + C_{11}^{(3b)}(K^2 + (K\pm 1)^2) \\ & \qquad \pm C_{11}^{(2)}(2K\pm 1)\Big]F_\pm(J,K). \end{aligned} \tag{6}$$

$C_{11}^{(1)}$ has a well-known expression in terms of molecular parameters [14], i.e.,

$$C_{11}^{(1)} = \frac{1}{2}\left[\left(\frac{v_5}{v_2}\right)^{1/2} + \left(\frac{v_2}{v_5}\right)^{1/2}\right]B_e\zeta_{2,5},$$

where $\zeta_{2,5} = \zeta_{2,5_b}^x = -\zeta_{2,5_a}^y$. Coriolis interaction of second order ($\Delta l = \mp 1, \Delta K = \pm 2$) between the $v_2 = 1$ and $v_5 = 1^{\pm 1}$ levels was expressed as

$$\begin{aligned} & \langle v_2 = 1, v_5 = 0, J, K|H|v_2 = 0, v_5 = 1, J, l = \mp 1, K\pm 2\rangle \\ & \quad = \pm\sqrt{2}\Big(C_{21}^{(2)} + C_{21}^{(3)}\Big)F_\pm(J,K)F_\pm(J,K\pm 1). \end{aligned} \tag{7}$$

The matrix elements of Eqs. (4)–(7) are given according to the phase conventions of Tarrago [15].

4. Spectral analysis

4.1. Description of the spectrum and assignments

Starting from the band centers and the rotational constants obtained for the $v_2 = 1$ and $v_5 = 1$ upper states and for the ground vibrational states of $CH_3{}^{79}Br$ and $CH_3{}^{81}Br$ in [10] and [16], respectively, it has been possible, using the set of programs written by Tarrago

and Delaveau [17] for C_{3v} symmetric-top molecules, to generate linelists for preliminary assignments. These assignments were then used to improve the upper state molecular constants and consequently the linelist prediction. As already shown by previous studies at low [9] and medium resolution [10], the v_2 and v_5 bands of CH_3Br have to be treated simultaneously because of the xy-Coriolis interaction between them. The improvement in the resolution by one order of magnitude allows us to see many new features; for example, the Q-branch lines are resolved in most cases (Fig. 3). The Q branches are found to be most illustrative for describing the observations, and they are generally used in the spectral examples given later in this paper.

The assignments in the v_2 band were started with the first $P_K(J)$ and $R_K(J)$ lines which show a regular K structure. The isotopic splitting in the $P_K(J)$ and $R_K(J)$ lines is observed for $J \geqslant 2$. As shown in Fig. 4, the P lines for v_2 with $K \geqslant 8$ are clearly shifted to lower frequencies while the situation is almost regular in the R side. In the v_2 band, for $CH_3{}^{79}Br$ and $CH_3{}^{81}Br$, we assigned 3037 lines with $K \leqslant 11$. Lines with $K > 11$ could not be found due to their weakness and J_{max} was around 68 on both the R and P sides.

The central part of the perpendicular band v_5 is presented in Fig. 2. The most striking feature in the spectrum is the sharpness of the ${}^RQ_0$ branch. This exceptional shape, centered at 1450.15 cm^{-1}, could be used for atmospheric detection. Q branches are well discernible and the separation between consecutive Q branches is about 11.8 cm^{-1}. As can be seen in Figs. 1 and 2, the lines of the v_5 band are weaker than those of the v_2 band,

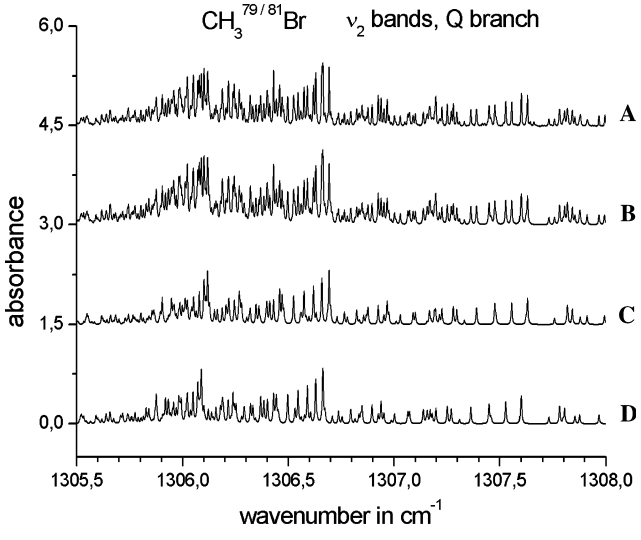

Fig. 3. The central part of the Q branch of the v_2 bands of $CH_3{}^{79}Br$ and $CH_3{}^{81}Br$. Trace (A) shows the observed spectrum, trace (B) shows the synthetic spectrum including both isotopomers, obtained by using the parameters of Model I. The lower traces (C) and (D) show the individual contributions of the two main isotopomers $CH_3{}^{79}Br$ and $CH_3{}^{81}Br$, respectively. For clarity, the spectra are shifted by 1.5.

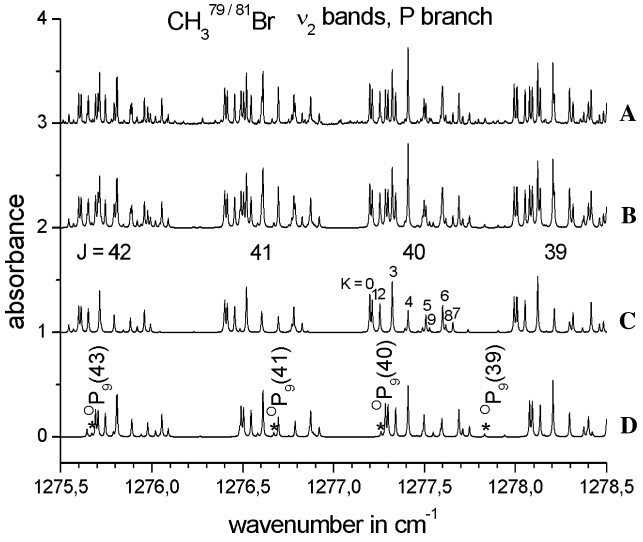

Fig. 4. Portion of the P branches of the v_2 bands of $CH_3{}^{79}Br$ and $CH_3{}^{81}Br$ near 1277.0 cm^{-1}: (A) observed spectrum, (B) synthetic spectrum including both isotopomers, (C) synthetic spectrum of $CH_3{}^{79}Br$, one can note the clusters with J range between 42 and 39 and the K-assignments of the ${}^QP_K(40)$, and (D) synthetic spectrum of $CH_3{}^{81}Br$. The perturbation-allowed transitions are indicated by asterisks.

except of the strong ${}^RQ_0$ branch. Some of them are comparable with those of the strongest lines of the $v_5 + v_3 - v_3$ "hot" band, centered at 1447.08 cm^{-1}, making the assignments very difficult in this region. In v_5, 4530 lines were assigned with $J \leqslant 63$ and $K \leqslant 8$, for both isotopomers.

The Coriolis interaction of second order ($\Delta l = \mp 1$, $\Delta K = \pm 2$) is most effective between $|v_5 = 1, l_5 = +1, K - 2\rangle$ and $|v_2 = 1, l_2 = 0, K\rangle$ because these two states are very close to each other as shown in Figs. 5 and 6. This resonance gives rise to perturbation-allowed transitions, indicated by asterisks in Fig. 4. The anomalous shape of the ${}^RQ_6$ branch presented in Fig. 7, compared to the normal ${}^PQ_3$ branch (Fig. 8) also nicely illustrates the existence of this perturbation which will be described in detail in the next section. All assignments were confirmed by the ground-state combination differences (GSCD), and no automatic assignment program was used. For the ground-state energy levels, we used the parameters from [16] listed in Table 1 and no attempt was made to fit the ground-state parameters again.

In the final fits, for $CH_3{}^{79}Br$, 430 line positions of v_5 taken from [11] (with $J_{max} \leqslant 65$ and $8 \leqslant K \leqslant 16$), and 3783 (3704) line positions obtained in this work of v_2 and v_5 (with $J_{max} \leqslant 68$ and $K_{max} \leqslant 11$) in the 1200–1650 cm^{-1} spectral region were fitted with a root-mean-square (RMS) deviation of 0.0007 (0.0006) cm^{-1}, respectively, for $CH_3{}^{79}Br$ and $CH_3{}^{81}Br$, which represents a significant improvement over previous studies. All the data set was weighted unity.

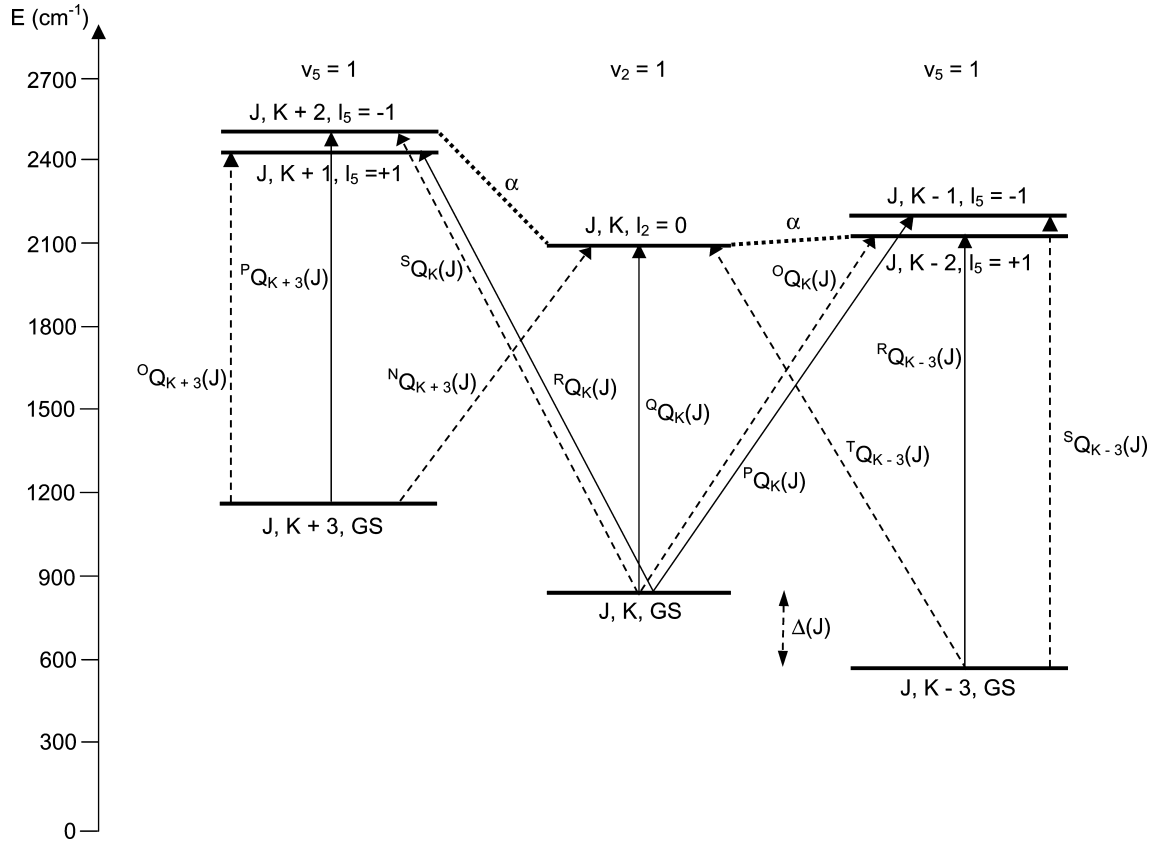

Fig. 5. Scheme showing how the Coriolis interaction, indicated by α give rise to perturbation-allowed transitions, shown by dashed lines. For the sake of simplicity, only Q-branch transitions are drawn.

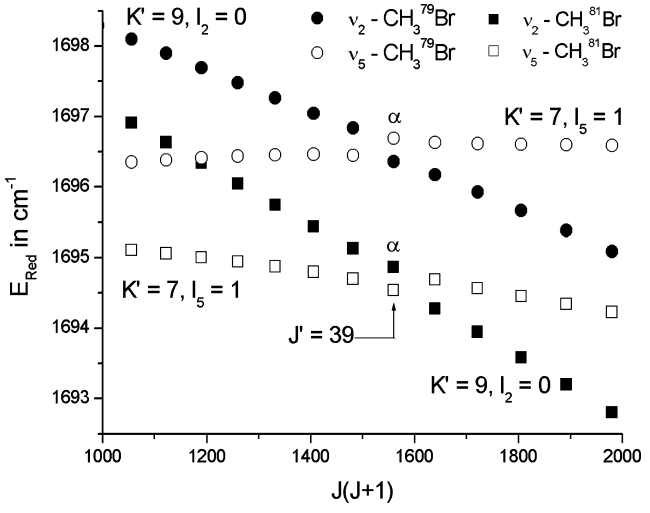

Fig. 6. Plot of the reduced energies $E_{\mathrm{red}}(J,K) = E(J,K) - B_0 J(J+1)$ of the v_2 $(K = 9, l_2 = 0)$ and the v_5 $(K = 7, l_5 = 1)$, showing the avoided crossing around $J = 39$ of levels linked by the $\Delta l = \mp 1, \Delta K = \pm 2$ interaction, indicated by α.

4.2. Description of applied models: reduced Hamiltonian

Two different but equivalent forms of reduced Hamiltonians with two different sets of constrained constants were applied according to Lobodenko's reduction [18,19]. The theory of the reduction of the effective Hamiltonian for Coriolis-interacting v_n (A_1) and v_t (E) fundamentals in C_{3v} molecules was developed by Lobodenko et al. [18], who applied it to the interpretation of the v_2 and v_5 bands of CH_3F. This theory has then been extended by Watson et al. [20], to include higher-order terms. Badaoui et al. [21] and Akkad et al. [22] applied Lobodenko's reduction, respectively, to the interpretation of the v_2/v_5 dyad of D_3SiF near 700 cm^{-1} and to the v_1/v_4 fundamental bands of $D_3Si^{35}Cl$ near 1600 cm^{-1}.

In our case, the Model I satisfies the conditions of Lobodenko's First Form. In that form, the Coriolis interaction parameter ζ_{nt} (related to $C_{11}^{(1)}$ as defined in Eq. (6)) has to be fixed to the value known from the harmonic force field and d_t, ζ_{nt}^{K}, and β_{nt} (related to our parameters d_3, $C_{11}^{(3b)}$, and $C_{21}^{(3)}$ as defined in Eqs. (5)–(7)) have to be fixed to the value zero. However, when trying to use in Model I the ab initio value of $C_{11}^{(1)} = 0.1915\,cm^{-1}$ obtained in the literature [23], no convergence could be obtained. The same problem was encountered by Badaoui et al. [21] in their study of the v_2/v_5 dyad of D_3SiF near 700 cm^{-1}. Like them we tried to contrain $C_{11}^{(1)}$ to different values in a small range, and found out that the minimum root-mean-square

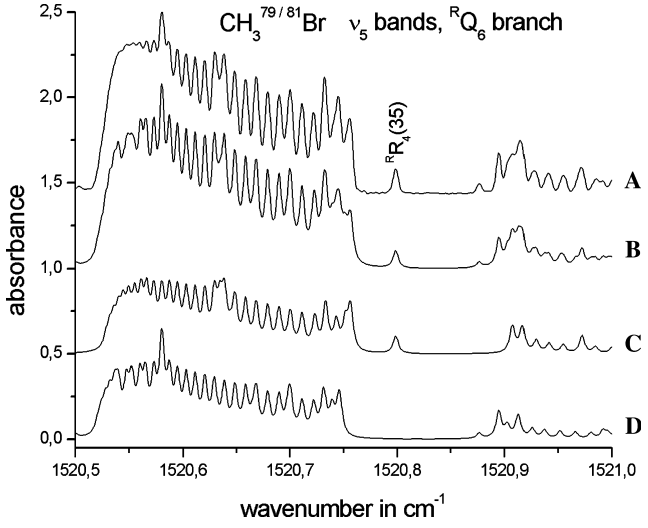

Fig. 7. The perturbed $^{R}Q_6$ branch of the v_5 bands of $CH_3{}^{79}Br$ and $CH_3{}^{81}Br$. Note the gap around 1520.75 cm^{-1}, due to a local perturbation with an avoided crossing around $J = 39$. Trace (A) shows the observed spectrum, trace (B) shows the synthetic spectrum including both isotopomers, obtained by using the parameters of Model I. The lower traces (C) and (D) show the individual contributions of the two main isotopomers $CH_3{}^{79}Br$ and $CH_3{}^{81}Br$, respectively.

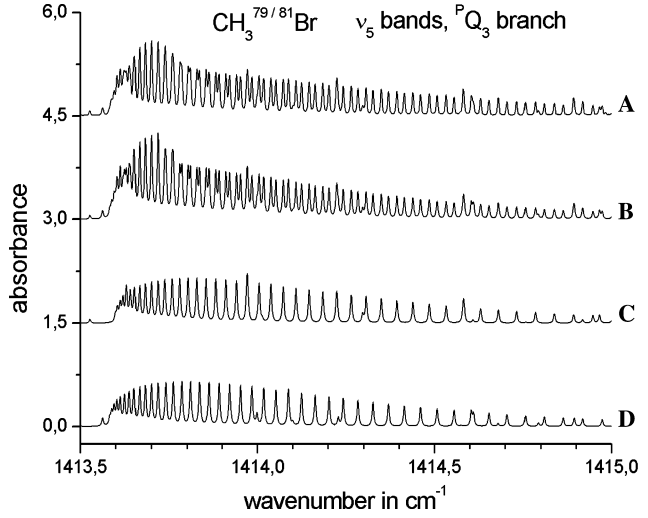

Fig. 8. The unperturbed $^{P}Q_3$ branch of the v_5 bands of $CH_3{}^{79}Br$ and $CH_3{}^{81}Br$. Trace (A) shows the observed spectrum, trace (B) shows the synthetic spectrum including both isotopomers, obtained by using the parameters of Model I. The lower traces (C) and (D) show the individual contributions of the two main isotopomers $CH_3{}^{79}Br$ and $CH_3{}^{81}Br$, respectively. For clarity, the spectra are shifted by 1.5.

deviation of our fit was obtained when $C_{11}^{(1)}$ is fixed to 0.1813 cm^{-1} for $CH_3{}^{79}Br$ and 0.1806 cm^{-1} for $CH_3{}^{81}Br$.

Model II obeys perfectly the Lobodenko's Second Form; i.e., q_t, d_t, α_{nt}^{BB}, and ζ_{nt}^{K} (related to our parameters q_5, d_3, $C_{21}^{(2)}$, and $C_{11}^{(3b)}$ as defined in Eqs. (4)–(7)) are fixed to the value zero. The α_{nt}^{AB} ($C_{11}^{(2)}$) resonance parameter fixed to zero in Model I is let free in the second model. The molecular parameters obtained in this work are reported in Tables 2–4. Both models show equivalent

Table 1
Ground-state constants of $CH_3{}^{79}Br$ and $CH_3{}^{81}Br$ from [16] (cm^{-1})[a]

Parameter	$CH_3{}^{79}Br$	$CH_3{}^{81}Br$
A_0	5.180632 (21)	5.180615 (11)
B_0	0.319160556 (3)	0.317947638 (2)
D_J^0 ($\times 10^7$)	3.2932 (2)	3.2694 (1)
D_{JK}^0 ($\times 10^6$)	4.2913 (4)	4.2640 (2)
D_K^0 ($\times 10^5$)	8.47 (4)	8.48 (2)
H_J^0 ($\times 10^{13}$)	−1.9 (4)	−1.9 (3)
H_{JK}^0 ($\times 10^{12}$)	3.2 (14)	4.7 (9)
H_{KJ}^0 ($\times 10^{10}$)	1.97 (2)	1.95 (2)
H_K^0 ($\times 10^9$)	4.1 (20)	4.6 (11)

[a] Errors in parentheses are 2.5 times the standard deviations in units of the last digit.

root-mean-square deviation for $CH_3{}^{79}Br$ and $CH_3{}^{81}Br$, demonstrating the internal coherence of our data.

Comparison with the parameters of [10] and [11] shows that we have improved the determination of all parameters. Two additional parameters were needed to describe the Coriolis-type interaction in our fits, namely a J-dependent term $C_{11}^{(3a)}$ and in Model I the second-order Coriolis interaction $C_{21}^{(2)}$. Using the parameters of Model I, synthetic spectra were calculated and are compared to observed spectra in Figs. 4 and 9. The agreement is excellent.

4.3. The interactions between A and E levels

Fig. 5 explains how forbidden transitions appear in this case. The Coriolis interaction of second order, with matrix elements in $\Delta(K - l_5) = \pm 3$, breaks down the usual selection rule $\Delta(K - l_5) = 0$, giving rise to perturbation-allowed ^{O}Q and ^{T}Q transitions (and their homologous $\Delta J = \pm 1$ transitions). The ^{N}Q and ^{S}Q transitions indicated on the left part of Fig. 5 are too weak to be observed because the interacting levels are rather far away. In addition, the effect of the second-order Coriolis interaction can be better illustrated with the help of a reduced upper state energy level diagram as done in Fig. 6. The avoided crossings which occur around $J = 39$ are indicated by α. This perturbation is also seen in Fig. 7 which shows the $^{R}Q_6$ branch of the v_5 bands of $CH_3{}^{79}Br$ and $CH_3{}^{81}Br$ with a gap around 1520.75 cm^{-1}.

4.4. Redetermination of A_0

From the observed dipole-allowed and perturbation-allowed transitions, the ground-state differences

$$\Delta(J) = E_0(J, K_1) - E_0(J, K_2) \tag{8}$$

can be derived. According to Eq. (1), they are

$$\begin{aligned}\Delta(J) = {} & (A_0 - B_0)(K_1^2 - K_2^2) - D_{JK}^0 J(J+1)(K_1^2 - K_2^2) \\ & - D_K^0(K_1^4 - K_2^4) + H_{JK}^0 J^2(J+1)^2(K_1^2 - K_2^2) \\ & + H_{KJ}^0 J(J+1)(K_1^4 - K_2^4) + H_K^0(K_1^6 - K_2^6). \end{aligned} \tag{9}$$

Table 2
Band centers and rotational constants for the v_2 and v_5 bands of $CH_3{}^{79}Br$: Models I and II

Constant	Model I						Model II			
	Ref. [10]		Ref. [11]		This work		Ref. [10]		This work	
	$v_2 = 1$	$v_5 = 1$	$v_2 = 1$	$v_5 = 1$	$v_2 = 1$	$v_5 = 1$	$v_2 = 1$	$v_5 = 1$	$v_2 = 1$	$v_5 = 1$
v_0	1305.9316 (4)	1442.9365 (3)	1305.9301 (7)	1442.9299 (6)	1305.928849 (57)	1442.931213 (44)	1305.9317 (3)	1442.9360 (3)	1305.928969 (58)	1442.931255 (44)
A	5.20162 (1)	5.13121 (2)	5.20177 (3)	5.13156 (4)	5.2024942 (32)	5.1320080 (22)	5.20162 (1)	5.13120 (2)	5.2024694 (36)	5.1320009 (23)
B	0.317938 (1)	0.3191988 (7)	0.317944 (3)	0.319218 (1)	0.317942836 (71)	0.319212907 (67)	0.318125 (1)	0.3191080 (6)	0.31811885 (24)	0.31912564 (13)
D_J ($\times 10^7$)	3.330 (3)	3.30228[a]	3.265 (7)	3.4054 (7)	3.30622 (75)	3.35200 (41)	3.331 (3)	3.30228[a]	3.30557 (86)	3.35183 (46)
D_{JK} ($\times 10^6$)	4.27962[a]	4.27962[a]	4.2908[a]	4.659 (8)	4.3026 (26)	4.6199 (17)	4.27962[a]	4.27962[a]	4.2688 (31)	4.6448 (19)
D_K ($\times 10^5$)	8.31[a]	8.31[a]	8.31[a]	7.63 (1)	8.7953 (29)	8.2559 (39)	8.31[a]	8.31[a]	8.7594 (38)	8.2312 (39)
H_J ($\times 10^{13}$)	—	—	—	—	−1.9[b]	−1.9[b]	—	—	−1.9[b]	−1.9[b]
H_{JK} ($\times 10^{12}$)	—	—	—	—	3.2[b]	3.2[b]	—	—	3.2[b]	3.2[b]
H_{KJ} ($\times 10^{10}$)	—	—	—	—	1.97[b]	3.236 (74)	—	—	1.97[b]	3.453 (78)
H_K ($\times 10^9$)	—	—	—	—	4.1[b]	8.199 (66)	—	—	4.1[b]	7.800 (68)
$(A\zeta)_5$		−1.21162 (5)		−1.21155 (8)		−1.2106858 (62)		−1.21160 (5)		−1.2106451 (62)
η_J ($\times 10^5$)		−1.28 (1)		−1.047 (18)		−1.1512 (11)		−1.38 (1)		−1.2120 (15)
η_K ($\times 10^4$)		−2.10 (3)		−2.84 (4)		−2.2084 (34)		−2.09 (3)		−2.2182 (34)
J_{max}/K_{max}	57/10	55/7	57/10	55/16	68/11	67/16	57/10	55/7	68/11	67/16
No. IR data		1507		651		4213		1505		4213
RMS (cm^{-1})		0.0035		0.0019		0.00073		0.0034		0.00073

Note. The results are in cm^{-1} and numbers in parentheses indicate 1σ in units of the last digit.
[a] Fixed to the ground-state value of [10].
[b] Fixed to the ground-state value of [16].

Table 3
Band centers and rotational constants for the v_2 and v_5 bands of $CH_3{}^{81}Br$: Models I and II

Constant	Model I				Model II			
	Ref. [10]		This Work		Ref. [10]		This work	
	$v_2 = 1$	$v_5 = 1$	$v_2 = 1$	$v_5 = 1$	$v_2 = 1$	$v_5 = 1$	$v_2 = 1$	$v_5 = 1$
v_0	1305.9025 (4)	1442.9242 (3)	1305.899488 (49)	1442.919224 (43)	1305.9025 (4)	1442.9238 (3)	1305.899503 (48)	1442.919095 (43)
A	5.20162 (1)	5.13112 (2)	5.2024843 (27)	5.1319377 (37)	5.20162 (1)	5.13111 (2)	5.2024704 (30)	5.1319765 (39)
B	0.316731 (2)	0.3179842 (7)	0.316735454 (63)	0.317997576 (62)	0.316916 (1)	0.3178940 (6)	0.31691163 (21)	0.31791022 (12)
D_J ($\times 10^7$)	3.300 (3)	3.2742[a]	3.28358 (75)	3.32554 (46)	3.280 (3)	3.2742[a]	3.28758 (82)	3.32279 (49)
D_{JK} ($\times 10^6$)	4.2438[a]	4.2438[a]	4.2883 (22)	4.5983 (16)	4.2438[a]	4.2438[a]	4.2690 (34)	4.6143 (22)
D_K ($\times 10^5$)	8.49[a]	8.49[a]	8.7989 (25)	8.2627 (80)	8.49[a]	8.49[a]	8.7763 (32)	8.3652 (82)
H_J ($\times 10^{13}$)	—	—	−1.9[b]	−1.9[b]	—	—	−1.9[b]	−1.9[b]
H_{JK} ($\times 10^{12}$)	—	—	4.7[b]	4.7[b]	—	—	4.7[b]	4.7[b]
H_{KJ} ($\times 10^{10}$)	—	—	1.95[b]	1.95[b]	—	—	1.95[b]	1.95[b]
H_K ($\times 10^9$)	—	—	4.6[b]	4.6[b]	—	—	4.6[b]	4.6[b]
$(A\zeta)_5$		−1.21116 (5)		−1.2101655 (56)		−1.21113 (5)		−1.2101344 (56)
η_J ($\times 10^5$)		−1.31 (1)		−1.1574 (11)		−1.40 (1)		−1.2291 (19)
η_K ($\times 10^4$)		−2.05 (3)		−2.2203 (33)		−2.03 (3)		−2.2259 (32)
J_{max}/K_{max}	57/10	55/7	64/11	61/8	57/10	55/7	64/11	61/8
No. IR data		1489		3704		1489		3702
RMS (cm^{-1})		0.0036		0.00062		0.0035		0.00060

Note. The results are in cm^{-1} and numbers in parentheses indicate 1σ in units of the last digit.
[a] Fixed to the ground-state value of [10].
[b] Fixed to the ground-state value of [16].

Table 4
"l"-Type and Coriolis-type interaction parameters of the v_2 and v_5 bands of $CH_3{}^{79}Br$ and $CH_3{}^{81}Br$

Interaction parameters	$CH_3{}^{79}Br$			$CH_3{}^{81}Br$	
	Ref. [10]	Ref. [11]	This work	Ref. [10]	This work
Model I					
q_5 ($\times 10^5$)	4.62 (4)	4.39 (8)	4.4169 (50)	4.58 (4)	4.3936 (44)
d_3	—	—	0[a]	—	0[a]
$C_{11}^{(1)}$	0.1807 (1)	0.1811 (2)	0.1813[a]	0.1800 (1)	0.1806[a]
$C_{11}^{(3a)}$ ($\times 10^7$)	—	—	−4.126 (70)	—	−4.279 (69)
$C_{11}^{(3b)}$	—	—	0[a]	—	0[a]
$C_{11}^{(2)}$ ($\times 10^3$)	—	—	0[b]	—	0[b]
$C_{21}^{(2)}$ ($\times 10^5$)	—	—	7.9255 (55)	—	7.8150 (50)
$C_{21}^{(3)}$	—	—	0[a]	—	0[a]
	Ref. [10]		This work	Ref. [10]	This work
Model II					
q_5 ($\times 10^5$)	—		0[a]	—	0[a]
d_3	—		0[a]	—	0[a]
$C_{11}^{(1)}$	0.19764 (7)		0.197254 (18)	0.19686 (7)	0.196608 (16)
$C_{11}^{(3a)}$ ($\times 10^7$)	—		−2.248 (73)	—	−2.777 (68)
$C_{11}^{(3b)}$	—		0[a]	—	0[a]
$C_{11}^{(2)}$ ($\times 10^3$)	0.783 (7)		0.7359 (10)	0.781 (6)	0.7420 (12)
$C_{21}^{(2)}$ ($\times 10^5$)	—		0[a]	—	0[a]
$C_{21}^{(3)}$	—		0[a]	—	0[a]

Note. The results are in cm^{-1} and numbers in parentheses indicate 1σ in units of the last digit.
[a] Constraint imposed by the chosen reduction.
[b] Fixed.

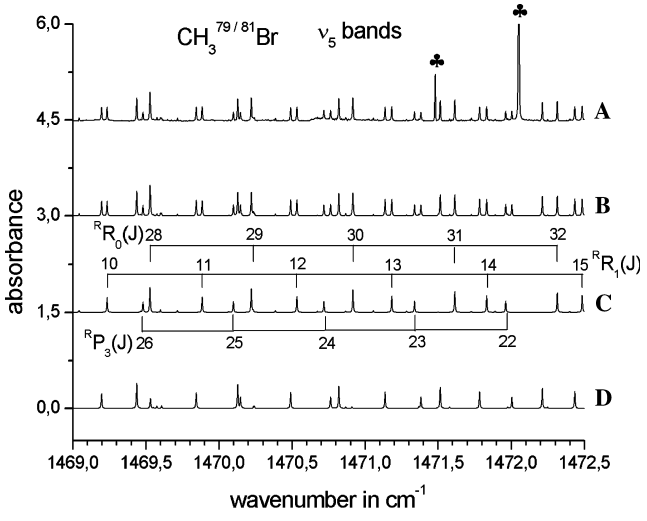

Fig. 9. A 3.5 cm^{-1} segment of the v_5 bands of $CH_3{}^{79}Br$ and $CH_3{}^{81}Br$. The J-assignments of the ${}^RR_0(J)$, ${}^RR_1(J)$, and ${}^RP_3(J)$ clusters are indicated. Trace (A) shows the observed spectrum, trace (B) shows the synthetic spectrum including both isotopomers, obtained by using the parameters of Model I. The lower traces (C) and (D) show the individual contributions of the two main isotopomers $CH_3{}^{79}Br$ and $CH_3{}^{81}Br$, respectively. For clarity, the spectra are shifted by 1.5. ♣ denotes the water vapor line.

These $\Delta(J)$ can be then separated in two parts:

$$\delta(J) = D_{JK}^0 J(J+1)(K_1^2 - K_2^2) - H_{JK}^0 J^2(J+1)^2(K_1^2 - K_2^2) - H_{KJ}^0 J(J+1)(K_1^4 - K_2^4) \quad (10)$$

and a purely K-dependent expression,

$$\Delta = \Delta(J) + \delta(J) = (A_0 - B_0)(K_1^2 - K_2^2) - D_K^0(K_1^4 - K_2^4) + H_K^0(K_1^6 - K_2^6). \quad (11)$$

Since the D_{JK}^0, H_{JK}^0, and H_{KJ}^0 constants, involved in Eq. (10), are well known from [16], the Δ values, which are independent of J, can be determined by forming the differences $\Delta(J)$ from the observations according to Eq. (8) and calculating the quantity $\delta(J)$ from Eq. (10). In our observations, $K_1 = 9$ (for v_2) and $K_2 = 6$ (for v_5).In deriving the $\Delta(J)$values from the observed wavenumbers, we only combined lines with the same $J' - J''$. Therefore the line separations give directly the differences $\Delta(J)$ in Eq. (8). The types of differences and the value Δ for each difference are given in Table 5. Employing the values of the parameters B_0, D_K^0, and H_K^0 from [16], given in Table 1 and using Eq. (11) we obtain:

Table 5
Different groups of observed differences for $CH_3{}^{79}Br$ and $CH_3{}^{81}Br$

Type of difference	$CH_3{}^{79}Br$		$CH_3{}^{81}Br$	
	N	Δ (cm^{-1})	N	Δ (cm^{-1})
${}^OP_9 - {}^RP_6$	5	218.32120 (41)	7	218.37577 (40)
${}^OR_9 - {}^RR_6$	3	218.32097 (26)	3	218.37687 (16)
${}^TR_6 - {}^QR_9$	2	218.32193 (6)	3	218.37664 (48)
Total	10	218.32129 (22)	13	218.37624 (25)

Note. N is the number of differences used and numbers in parentheses indicate 1σ in units of the last digit.

Table 6
Ground-state axial rotational constant for $CH_3{}^{79}Br$ and $CH_3{}^{81}Br$ (cm^{-1}): comparison with previous studies

Constant	$CH_3{}^{79}Br$			$CH_3{}^{81}Br$		
	Ref. [10]	Ref. [16]	This work	Ref. [10]	Ref. [16]	This work
A_0	5.1801[a]	5.180632 (21)[b]	5.1806104 (49)[c]	5.1802 (2)[c]	5.180615 (11)[b]	5.1806251 (55)[c]

[a] This value was obtained by only one observation.
[b] Numbers in parentheses are 2.5 times the standard deviations in units of the last digit.
[c] Numbers in parentheses indicate 1 in units of the last digit.

$A_0 = 5.1806104\ (49)$ for $CH_3{}^{79}Br$

and

$A_0 = 5.1806251\ (55)$ for $CH_3{}^{81}Br$.

These constants are listed in Table 6 together with the previously determined values. A comparison between present and previous values of A_0 shows slight discrepancies, particularly with [10]. However, our values are more accurate but in agreement with [16], taking into account their uncertainties.

It is interesting to note that, for the first time, the isotopic difference between the A_0 constants of $CH_3{}^{79}Br$ and $CH_3{}^{81}Br$ have been observed with sufficient accuracy to be significant. The interpretation of this observation is straightforward: the ground-state rotational constants are isotopically dependent via the vibrational dependence of the rotational constants, usually written as

$$A_0 = A_e - \sum_i \alpha_i^A d_i/2, \tag{12}$$

where d_i is the degeneracy of the vibration v_i and α_i^A the difference between the constants of the ground state and the first excited state. At equilibrium, the A_e constants for $CH_3{}^{79}Br$ and $CH_3{}^{81}Br$ are equal. Then using Eq. (12), the difference

$$^{81}A_0 - {}^{79}A_0 = \sum_i \left({}^{79}\alpha_i^A - {}^{81}\alpha_i^A\right) d_i/2 \tag{13}$$

can be obtained. By using the α_i^A constants given in Table 7, the following value for the A_0 difference is derived:

Table 7
α_i^A and α_i^B values for $CH_3{}^{79}Br$ and $CH_3{}^{81}Br$ ($10^{-3}\ cm^{-1}$)

	$CH_3{}^{79}Br$	$CH_3{}^{81}Br$	Ref.
α_i^A			
α_1^A	53.99 (4)	53.95 (4)	[24]
α_2^A	−21.862 (24)	−21.869 (14)	This work
α_3^A	7.2875 (17)	7.2676 (19)	[25]
α_4^A	28.738 (4)	28.707 (4)	[26]
α_5^A	48.624 (22)	48.677 (15)	This work
α_6^A	−29.521 (23)	−29.518 (12)	[8]
α_i^B			
α_1^B	0.009 (1)	0.006 (1)	[24]
α_2^B	1.217720 (74)	1.212184 (65)	This work
α_3^B	2.42667 (6)	2.41234 (7)	[25]
α_4^B	−0.1970 (2)	−0.1965 (2)	[26]
α_5^B	−0.052351 (70)	−0.049938 (64)	This work
α_6^B	1.139376 (33)	1.134768 (22)	[8]

$^{81}A_0 - {}^{79}A_0 = 0.9\ (49) \times 10^{-5}\ cm^{-1}$. This is in agreement with the value of $^{81}A_0 - {}^{79}A_0 = 1.5\ (10) \times 10^{-5}\ cm^{-1}$ obtained from the present study.

4.5. Calculation of A_e and B_e values

Using Eq. (12) and a similar equation for B_e, i.e.,

$$B_e = B_0 + \sum_i \alpha_i^B d_i/2 \tag{14}$$

and using the α_i data from Table 7, the A_0 values obtained in this work, and B_0 values from [16] (Table 1), we can derive the following accurate A_e and B_e values:

$A_e = 5.24814\ (9)$, $\quad B_e = 0.3218773\ (9)$ for $CH_3{}^{79}Br$

and

$A_e = 5.24817\ (6)$, $\quad B_e = 0.3206512\ (9)$ for $CH_3{}^{81}Br$.

Table 8 compares our equilibrium constants to the values determined previously. One can note the good agreement between our values and those of [10].

The percentage difference between our values and the ab initio calculated equilibrium constants of [27] is less than 3%.

4.6. Integrated band intensities, dipole moment derivatives, and intensity perturbation

The integrated band intensities of the v_2 and v_5 fundamentals have been measured previously at low spectral resolution ($S_2 = 62.5\ (2.3)\ cm^{-2}\ atm^{-1}$ and $S_5 = 51.1\ (2.3)\ cm^{-2}\ atm^{-1}$, at 296 K) [28]. The transition moments have been adjusted ($d_2 = \partial\mu/\partial q_2 = 0.0703$ D and $d_5 = \partial\mu/\partial q_5 = 0.0427$ D) to reproduce correctly these values. The values we derived from our prediction for the sum of all intensities at 296 K are: $S_2 = 61.38\ cm^{-2}\ atm^{-1}$ and $S_5 = 50.46\ cm^{-2}\ atm^{-1}$, respectively, for the v_2 and v_5 bands of CH_3Br. The percentage difference between our values and those of [28] is less than 2% for the two bands. The absolute value of the ratio of the dipole moment derivatives of the v_2 and v_5 bands of CH_3Br is $|d_2/d_5| = 1.65$.

Using the parameters of Model I, synthetic spectra (Fig. 10) were calculated to show the effect of changing the sign (Figs. 10A and B) of the intensity perturbation ($d_2 \times \zeta_{25} \times d_5$). Comparison with the observed spectrum leads to the conclusion that the intensity perturbation is positive.

Table 8
Comparison of experimental and ab initio equilibrium values (A_e, B_e) of $CH_3{}^{79}Br$ and $CH_3{}^{81}Br$

Equilibrium constants	$CH_3{}^{79}Br$		$CH_3{}^{81}Br$		CH_3Br
	Ref. [10]	This work	Ref. [10]	This work	Ab initio, Ref. [27]
A_e	5.2471 (11)	5.24814 (9)	5.2470 (9)	5.24817 (6)	5.3041
B_e	0.321891 (5)	0.3218773 (9)	0.320667 (5)	0.3206512 (9)	0.3150

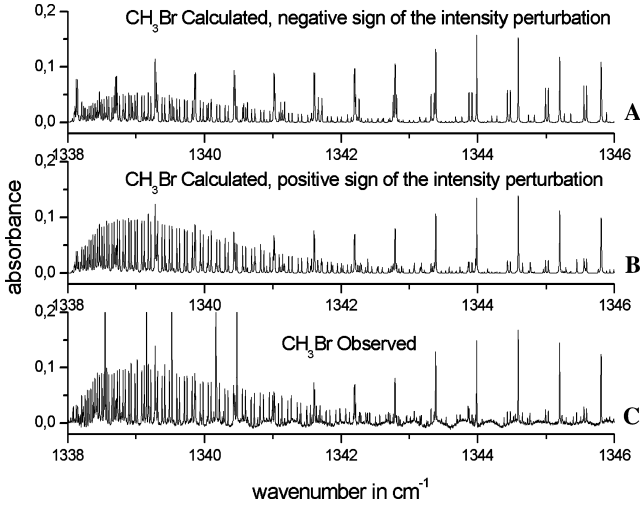

Fig. 10. Effect of the change of the sign of the intensity perturbation on the calculated spectra: comparison with observed spectrum. The simulations were made with the parameters of Model I and values $d_2/d_5 = -1.65, +1.65$, for traces (A) and (B). Strong lines in the observed spectrum, trace (C), which are not reproduced by the simulations are water lines.

5. Discussion

5.1. Comparison with literature data

The present contribution on the $v_2 = 1$ and $v_5 = 1$ states of $CH_3{}^{79}Br$ and $CH_3{}^{81}Br$ may be compared with previous study [10] in which transitions measured with a resolution of $0.015\,cm^{-1}$ were fitted to 12 parameters. The standard deviation of their fit, $0.0035\,cm^{-1}$, is larger than the present one by a factor of 5, clearly due to the significantly higher resolution of the present study.

Moreover, it is important to note that the value of the Coriolis coupling term $C_{11}^{(1)}$ is slightly different for $CH_3{}^{79}Br$ and $CH_3{}^{81}Br$. It is possible to deduce a value for $\zeta_{2,5}$ from $C_{11}^{(1)}$ as was seen earlier, using the B_e value obtained in this work for each isotopic species:

$\zeta_{2,5} = 0.6121 \pm 0.0006$ for $CH_3{}^{79}Br$

$\zeta_{2,5} = 0.6124 \pm 0.0005$ for $CH_3{}^{81}Br$.

Anttila et al. [10] published a quantity $W_{cor} = \sqrt{2}C_{11}^{(1)}$, from which one can deduce the value of $\zeta_{2,5} = 0.613$, for $CH_3{}^{79}Br$ and $CH_3{}^{81}Br$. This value is in good agreement with the present one. On the other hand, they also give $W_{l(2,2)} = -9.23\ (7) \times 10^{-5}\,cm^{-1}$ for $CH_3{}^{79}Br$ and $W_{l(2,2)} = -9.16\ (8) \times 10^{-5}\,cm^{-1}$ for $CH_3{}^{81}Br$, which can be converted into $q_5 = -W_{l(2,2)}/2 = 4.62\ (4) \times 10^{-5}\,cm^{-1}$ and $4.58\ (4) \times 10^{-5}\,cm^{-1}$, respectively, for $CH_3{}^{79}Br$ and $CH_3{}^{81}Br$, in reasonable agreement with the values of Table 4. Ouahman et al. [11] gave $4.39\ (8) \times 10^{-5}\,cm^{-1}$ for q_5, very close to our value. For all parameters, the agreement with [11] is within a few percentage.

In [10], the authors did not determine the Coriolis interaction of the second order. But their estimated value is $\gamma = C_{21}^{(2)} = 7.8 \times 10^{-5}\,cm^{-1}$, in agreement with those obtained in Model I for $CH_3{}^{79}Br$ and $CH_3{}^{81}Br$, from our calculations. They also published a quantity $W_2 = \sqrt{2}C_{11}^{(2)} = 1.107 \pm 0.008$ for $CH_3{}^{79}Br$ and $1.104 \pm 0.006\,cm^{-1}$ for $CH_3{}^{81}Br$, from which one can deduce the value of $C_{11}^{(2)} = 0.783 \pm 0.007\,cm^{-1}$ for

Table 9
Comparison of experimental parameters (cm^{-1}) from Models I and II with ab initio predictions[a]

Parameters	$CH_3{}^{79}Br$		$CH_3{}^{81}Br$		CH_3Br	
	Model I	Model II	Model I	Model II	Ab initio, Ref. [23]	Ab initio, Ref. [27]
v_2	1305.928849	1305.928969	1305.899488	1305.899503	1317	—
v_5	1442.931213	1442.931255	1442.919224	1442.919095	1445	—
α_2^A ($\times 10^3$)	−21.862	−21.837	−21.869	−21.855	—	−22.758
α_5^A ($\times 10^3$)	48.624	48.631	48.677	48.639	—	44.377
α_2^B ($\times 10^3$)	1.217720	1.041706	1.212184	1.036008	—	0.971*
α_5^B ($\times 10^3$)	−0.052351	0.034916	−0.049938	0.037418	—	−0.014*
$A\zeta_5$	−1.2106858	−1.2106451	−1.2101655	−1.2101344	—	—
$q_5\times$ ($\times 10^5$)	4.4169	0[b]	4.3936	0[b]	—	5.35*
$C_{11}^{(1)}$	0.1813[b]	0.197254	0.1806[b]	0.196608	0.1915	—
$(\alpha_2^B + 2\alpha_5^B)$ ($\times 10^3$)	1.113	1.112	1.112	1.111	—	0.943*
$(\eta_5^J + \eta_5^K)$ ($\times 10^5$)	−23.235	−23.394	−23.360	−23.488	—	—

[a] Starred values do not contain contributions of the v_2/v_5 Coriolis resonance.
[b] Constraint imposed by the chosen reduction.

$CH_3{}^{79}Br$ and $C_{11}^{(2)} = 0.781 \pm 0.006\,cm^{-1}$ for $CH_3{}^{81}Br$, in agreement with those obtained in the present work.

Thanks to the increase of the quantum number range, the distortion constants, which were constrained for the majority to those of the ground state in previous studies [9–11] are determined here.

Comparing the experimental results of the present study with some ab initio calculations of [23] and [27], we find moderate agreement with respect to α_2^A and α_5^A as shown in Table 9. The calculated harmonic wavenumbers v_i are in good agreement with the experimental ones. But for the parameters α_2^B, α_5^B, and q_5, our results disagree with ab initio values. Indeed in the ab initio values, no contribution of the v_2/v_5 Coriolis resonance was taken into account. The sum $\alpha_2^B + 2\alpha_5^B$ remains independent of the model and, differs by 15%, from the ab initio sum.

5.2. Comparison of Models I and II

The comparison of Models I and II shows a good agreement for the parameters v_2, v_5, α_2^A, α_5^A, α_2^B, and $A\zeta_5$. For both models, and both isotopomers, the quartic centrifugal distortion constants are not too different from their values of the ground state. The highest difference (8%) is observed for $D_{JK}^0 - D_{JK}^5$. Let us note that CH_3Br is the unique methyl halide for which α_5^B exhibits a sign reversal when we change from Model I to Model II. We note also that α_5^B is very small, like α_1^B. This difference in size and in sign appear also on the quantity $\alpha_5^B + 1/2q_5$. The values of $\alpha_5^B + 1/2q_5$, obtained for Models I and II are, respectively, -3.027 and 3.492×10^{-5} for $CH_3{}^{79}Br$ and -2.797 and 3.742×10^{-5} for $CH_3{}^{81}Br$. Anttila et al. [10], obtained -1.50 and 5.27×10^{-5} for $CH_3{}^{79}Br$ and -1.36 and 5.37 for $CH_3{}^{81}Br$, respectively, for Models I and II. The other relations between molecular parameters ($\alpha_2^B + 2\alpha_5^B$ and $\eta_5^J + \eta_5^K$) which are invariant to the reduction are established here. Table 9 reported the values obtained in the present work.

6. Conclusions

A high-resolution Fourier transform spectrum covering the 900–2000 cm^{-1} spectral range has been used to perform an extensive analysis of the v_2 and v_5 bands of $CH_3{}^{79}Br$ and $CH_3{}^{81}Br$. Then, using a Hamiltonian matrix which takes into account explicitly both the Coriolis interactions (first and second order) and the $l(2,2)$ resonance in the v_5 band, it has been possible to perform an accurate prediction of P, Q, and R lines of both v_2 and v_5 bands of $CH_3{}^{79}Br$ and $CH_3{}^{81}Br$, improving significantly upon previous analysis. The axial rotational constants A_0 were redetermined from allowed and perturbation-allowed infrared transitions observed in the v_2 and v_5 bands around the local crossing. The values obtained for both isotopomers are in good agreement with those obtained previously [16], but much more accurate. New accurate equilibrium constants A_e and B_e have been evaluated for $CH_3{}^{79}Br$ and $CH_3{}^{81}Br$. The ratio of the transition moments, $|d_2/d_5| = 1.65$, and a positive sign of the Coriolis intensity perturbation have been determined.

The v_2 and v_5 bands of CH_3Br are not located in a clean atmospheric window because of telluric water absorption. However, some features of the strong v_5 band, compared to the v_6 band ($S_6^0 = 26.60$ (9) $cm^{-2}\,atm^{-1}$) [8], might be observed. Due to its great intensity, the sharp $^RQ_0$ branch of the v_5 band, centered at 1450.15 cm^{-1}, could be used for this purpose. A table with line positions and intensities is available upon request to authors.

Acknowledgments

We dedicate this paper to Jon T. Hougen to thank him for all his encouragements along the years and numerous scientifical advices. One of us (F. Kwabia Tchana), would like especially to express his gratitude to Jon Hougen who taught us a class last spring in France and with a few words, enabled us to understand the necessity of the group theory in molecular spectroscopy. This study was supported by the Programme National de Chimie Atmosphérique (PNCA). The authors thank the Ministère des Affaires Etrangères (Service de Coopération et d'Action Culturelle à l'Ambassade de France au Cameroun) and the Agence Universitaire de la Francophonie (Bureau Afrique Centrale, Cameroun) for financial support. The authors are grateful to G. Tarrago, who kindly provided her codes for calculation of frequencies and intensities of C_{3v} symmetric-top molecules. It is a pleasure to thank N. Bensari-Zizi who provided us with assignments of line positions of $CH_3{}^{79}Br$ between 1520 and 1650 cm^{-1}. The referee of this paper is acknowledged for many helpful suggestions and comments.

References

[1] J.H. Butler, Geophys. Res. Lett. 21 (1994) 185.
[2] R.J. Cicerone, Science 263 (1994) 1243.
[3] World Meteorological Organization (WMO), "Scientific Assessment of Ozone Depletion: 1998," Report 44, WMO Global Ozone Research and Monitoring Project, Chapter 2, Geneva, Switzerland, 1999.
[4] O.W. Wingenter, B.C. Sive, D.R. Blake, F. Sherwood Rowland, B.A. Ridley, Geophys. Res. Lett. 30 (2003) 2160.
[5] C. Di Lauro, I.M. Mills, J. Mol. Spectrosc. 21 (1966) 386.
[6] Y. Morino, C. Hirose, J. Mol. Spectrosc. 24 (1967) 204.
[7] G. Graner, J. Mol. Spectrosc. 90 (1981) 394.
[8] E. Brunetaud, I. Kleiner, N. Lacome, J. Mol. Spectrosc. 216 (2002) 30.
[9] G. Graner, W.E. Blass, J. Phys. (Orsay, France) 36 (1975) 769.
[10] R. Anttila, C. Betrencourt-Stirnemann, J. Dupré, J. Mol. Spectrosc. 100 (1983) 54.

[11] M. Ouahman, N. Ben Sari-Zizi, C. Alamichel, Spectrochim. Acta A 45 (1989) 175.
[12] R.A. Toth, J. Opt. Soc. Am. B 8 (1991) 2236.
[13] D. Papousek, M.R. Aliev, Molecular Vibrational–Rotational Spectroscopy, Elsevier, Amsterdam/New York, 1982.
[14] G. Tarrago, K. Narahari Rao, L.W. Pinkley, J. Mol. Spectrosc. 79 (1980) 31.
[15] G. Tarrago, Cah. Phys. 19 (1965) 149.
[16] J. Sakai, M. Katayama, J. Mol. Struct. 190 (1988) 113.
[17] G. Tarrago, M. Delaveau, J. Mol. Spectrosc. 119 (1986) 418.
[18] E.I. Lobodenko, O.N. Sulakshina, V.I. Perevalov, V.L.G. Tyuterev, J. Mol. Spectrosc. 126 (1987) 159.
[19] K. Sarka, D. Papousek, J. Demaison, H. Mäder, H. Harder, in: D. Papousek (Ed.), Vibration–Rotational Spectroscopy and Molecular Dynamics, World Scientific, Singapore, 1997, p. 166.
[20] J.K.G. Watson, C. Gerke, H. Harder, K. Sarka, J. Mol. Spectrosc. 187 (1998) 131.
[21] M. Badaoui, N. Ben Sari-Zizi, G. Graner, E.B. Mkadmi, H. Bürger, P. Pracna, J. Mol. Spectrosc. 200 (2000) 72.
[22] K. Akkad, N. Ben Sari-Zizi, H. Bürger, E.B. Mkadmi, J. Mol. Spectrosc. 213 (2002) 35.
[23] W. Schneider, W. Thiel, J. Chem. Phys. 86 (1987) 923.
[24] M. Betrencourt, M. Morillon-Chapey, C. Amiot, G. Guelachvili, J. Mol. Spectrosc. 57 (1975) 402.
[25] R. Lakanen, M. Koivusaari, V.-M. Horneman, J. Kauppinen, J. Mol. Spectrosc. 135 (1989) 188.
[26] C. Betrencourt-Stirnemann, G. Graner, G. Guelachvili, J. Mol. Spectrosc. 51 (1974) 216.
[27] W. Schneider, W. Thiel, Chem. Phys. 159 (1992) 49.
[28] C. Anastasi, A.E. Heathfield, G.P. Knight, F. Nicolaisen, Spectrochim. Acta Part A 50 (1994) 1791.